Enhanced synthesis of saturated phospholipids is associated with ER stress and lipotoxicity in palmitate-treated hepatic cells[S]

Alexandra K. Leamy,* Robert A. Egnatchik,* Masakazu Shiota,† Pavlina T. Ivanova,§ David S. Myers,§ H. Alex Brown,§,,†† and Jamey D. Young[1],*,†**

Department of Chemical and Biomolecular Engineering,* Department of Molecular Physiology and Biophysics,† Department of Pharmacology, Vanderbilt University Medical Center,§ Department of Biochemistry,** and Vanderbilt Institute of Chemical Biology,†† Vanderbilt University, Nashville, TN 37235-1604

Abstract **High levels of saturated FAs (SFAs) are acutely toxic to a variety of cell types, including hepatocytes, and have been associated with diseases such as type 2 diabetes and nonalcoholic fatty liver disease. SFA accumulation has been previously shown to degrade endoplasmic reticulum (ER) function leading to other manifestations of the lipoapoptotic cascade. We hypothesized that dysfunctional phospholipid (PL) metabolism is an initiating factor in this ER stress response. Treatment of either primary hepatocytes or H4IIEC3 cells with the SFA palmitate resulted in dramatic dilation of the ER membrane, coinciding with other markers of organelle dysfunction. This was accompanied by increased de novo glycerolipid synthesis, significant elevation of dipalmitoyl phosphatidic acid, diacylglycerol, and total PL content in H4IIEC3 cells. Supplementation with oleate (OA) reversed these markers of palmitate (PA)-induced lipotoxicity. OA/PA cotreatment modulated the distribution of PA between lipid classes, increasing the flux toward triacylglycerols while reducing its incorporation into PLs. Similar trends were demonstrated in both primary hepatocytes and the H4IIEC3 hepatoma cell line.[JLR] Overall, these findings suggest that modifying the FA composition of structural PLs can protect hepatocytes from PA-induced ER stress and associated lipotoxicity.**—Leamy, A. K., R. A. Egnatchik, M. Shiota, P. T. Ivanova, D. S. Myers, H. A. Brown, and J. D. Young. **Enhanced synthesis of saturated phospholipids is associated with ER stress and lipotoxicity in palmitate-treated hepatic cells.** ***J. Lipid Res.*** **2014.** 55: **1478–1488.**

Supplementary key words saturated fatty acids • lipoapoptosis • nonalcoholic fatty liver disease • endoplasmic reticulum stress • phospholipid metabolism • membrane composition • triacylglycerol synthesis

FFAs are involved in a diverse range of functions within hepatic cells, including esterification into triacylglycerols (TAGs); oxidation to fuel mitochondrial metabolism, synthesis, and remodeling of phospholipids (PLs); and conversion to signaling molecules such as prostaglandins or leukotrienes. The effects of elevated FFAs have been previously studied in cultured hepatic cell lines as a model for recapitulating the lipotoxicity that has been observed in obese type 2 diabetes and nonalcoholic fatty liver disease (NAFLD) (1–5). In these disease states, ectopic accumulation of FFAs in nonadipose tissues such as liver, pancreas, and skeletal muscle can interfere with normal cellular function and induce apoptotic cell death. These lipotoxic effects have shown dependence on FA chain length and saturation. Exposure to long-chain saturated FAs (SFAs), such as palmitate (PA) or stearate, leads to lipoapoptosis in many cell types including hepatocytes (2, 6, 7). In contrast, MUFAs, such as oleate (OA), are not acutely cytotoxic to hepatic cells and have been shown to exert a protective effect when combined with toxic loads of SFAs (8–10).

The mechanism by which metabolism of specific lipid species results in apoptosis has not been fully elucidated.

This work was supported by National Science Foundation (NSF) CAREER Award CBET-0955251 (J.D.Y.). R. A. Egnatchik was supported by the NSF Graduate Research Fellowship Program. M. Shiota was supported by National Institutes of Health Grant DK060667. Partial support for the work was also provided by National Institutes of Health Grant U54 GM69338 (H.A.B.). Fatty acyl lipid analysis was performed by the Vanderbilt Diabetes Research and Training Center's Hormone Assay Core, which is supported by National Institutes of Health Grant DK020593. Electron microscopy was performed in part through the use of the Vanderbilt University Medical Center Cell Imaging Shared Resource, supported by National Institutes of Health Grants CA68485, DK20593, DK58404, HD15052, DK59637, and EY08126.

Manuscript received 21 April 2014 and in revised form 21 May 2014.

Published, JLR Papers in Press, May 23, 2014
DOI 10.1194/jlr.M050237

Abbreviations: CHO, Chinese hamster ovary; CHOP, CCAAT/enhancer binding protein homologous protein; DAG, diacylglycerol; ER, endoplasmic reticulum; GC-FID, GC-flame ionization detection; LPA, lysophosphatidic acid; NAFLD, nonalcoholic fatty liver disease; OA, oleate; PA, palmitate; PC, phosphatidylcholine; PL, phospholipid; PtdOH, phosphatidic acid; SFA, saturated FA; TAG, triacylglycerol; TEM, transmission electron microscopy; UFA, unsaturated FA; UPR, unfolded protein response.

[1]To whom correspondence should be addressed.
e-mail: j.d.young@vanderbilt.edu

[S] The online version of this article (available at http://www.jlr.org) contains supplementary data in the form of one table and five figures.

A prior in vivo study demonstrated the deleterious effects of increased dietary saturated fat by feeding mice a so-called "fast-food diet" that was high in saturated fat and cholesterol. These mice developed pathological symptoms of nonalcoholic steatohepatitis (NASH), in contrast to mice fed a typical high-fat diet that only developed simple steatosis without NASH symptoms (11). In vitro lipotoxicity experiments in a variety of cell lines, including Chinese hamster ovary (CHO) cells (10, 12, 13), pancreatic β cells (14, 15), breast cancer cells (16), and hepatic cells (6, 9, 17–19), have shown that SFA overexposure is characterized by expression of proinflammatory cytokines, endoplasmic reticulum (ER) impairment, elevated reactive oxygen species (ROS), and eventual apoptosis without significant TAG formation. In contrast, MUFAs and PUFAs induce substantial TAG formation but do not initiate apoptosis (6, 10). These findings suggest that lipotoxicity does not correlate with accumulation of TAGs containing unsaturated FAs (UFAs), and that other lipid classes may mediate responses to SFA overload. Ceramide accumulation has been postulated as a major contributing factor in palmitate-induced lipotoxicity due to the fact that PA and serine are substrates for de novo ceramide biosynthesis. Although previous work has demonstrated the ability of ceramides to activate apoptotic signaling in muscle cells (20), recent studies have shown that SFAs promote ER stress (13, 17) and ROS accumulation (10) independently of ceramide synthesis in CHO and hepatic cells. Therefore, identifying specific lipid metabolites that induce lipotoxicity in hepatic cells, as well as strategies to circumvent them by diverting SFAs into nontoxic disposal pathways, represents a potential research area for prevention and treatment of NAFLD.

Markers of ER stress, including CCAAT/enhancer binding protein homologous protein (CHOP) and depletion of Ca^{2+} stores from the ER lumen, appear soon after exposure to SFAs but are not found in cells treated with MUFAs (21). ER Ca^{2+} depletion has been shown to occur in a range between 1 and 4 h following SFA exposure (8, 13), indicating that the initial metabolism of SFA results in rapid perturbations to ER homeostasis and initiation of the compensatory ER stress pathway known as the unfolded protein response (UPR). Aberrant lipid metabolism has been previously linked to disruptions in ER homeostasis leading to chronic ER stress in obesity (22). Based on this recent literature, we hypothesized that dysfunctional PL metabolism and subsequent changes to FA composition of membrane lipid species may play a critical role in initiating ER stress under conditions of lipotoxicity. The composition of the ER membrane typically contains unsaturated phosphatidylcholine (PC) as its major PL component (23). This allows the ER to maintain a high degree of fluidity in order to carry out its critical role in preserving proper protein folding and trafficking. The degree of saturation of PLs plays an important role in many membrane-associated functions and homeostasis. Abnormal incorporation of saturated PL species can result in detrimental stiffening of cellular membranes and loss of function (24). Relatively small changes in ER homeostasis can result in the induction of UPR and reduced capacity to transport calcium (25, 26). Therefore, even limited incorporation of SFAs into PL species, particularly PC, could be detrimental to ER function and lead to the increased UPR signaling observed in response to SFA overexposure.

In the present study, we investigated the mechanisms by which upstream SFA metabolism induces hepatic cell lipotoxicity in both the H4IIEC3 rat hepatoma cell line and freshly isolated primary hepatocytes. We demonstrated that exogenous PA induces dramatic and rapid alterations in ER morphology, indicative of compromised ER integrity confirmed by high-resolution cellular imaging with transmission electron microscopy (TEM). PA treatment resulted in dramatic increases in 16:0 lysophosphatidic acid (LPA) and dipalmitoyl phosphatidic acid (32:0 PtdOH), suggesting de novo lipid biosynthesis via the Kennedy pathway (27). Diacylglycerols (DAGs) also show incorporation of PA and further conversion preferentially into membrane PLs as opposed to TAGs. The resulting changes in PL acyl chain composition are associated with an increase in markers of ER stress and characteristic indicators of lipotoxicity (mitochondrial dysfunction, caspase activation, and cell death). Cotreatment with OA was found to suppress dysfunction and dilation of the ER membrane, reduce PA incorporation into PLs, and restore overall membrane saturation. Supplementing PA-treated cells with varying concentrations of OA almost completely abolished 16:0 LPA and 32:0 PtdOH accumulations and rerouted DAG species away from PL synthesis and into TAG esterification. Reduction in markers of ER stress and lipotoxicity were observed in those cases. To our knowledge, this is the first time that changes in PL synthesis, PL FA composition, and ER membrane structure have been directly linked to lipotoxicity initiation in hepatic cells. We demonstrate that MUFA supplementation reduces PA incorporation into PL species and restores a more balanced saturated:unsaturated membrane PL composition while increasing metabolic flux toward more benign TAG synthesis.

EXPERIMENTAL PROCEDURES

Materials and reagents

Oleic and palmitic acids, BSA, and DMEM were all purchased from Sigma-Aldrich (St. Louis, MO). CHOP primary (mouse) and goat anti-mouse secondary antibodies were purchased from Abcam (Cambridge, MA). β-Actin primary (goat) and donkey anti-goat secondary antibodies were procured from Santa Cruz Biotechnology Inc. (Santa Cruz, CA). All other chemicals were purchased from standard commercial sources.

Preparation of FA solutions

FA treatment solutions were prepared by coupling FFAs to BSA. Specifically, palmitate or oleate was fully dissolved in 200-proof ethanol for a concentration of 195 mM. This FFA stock solution was added to a prewarmed BSA solution (10% w/w, 37°C) for a final FFA concentration of 3 mM, ensuring that the concentration of ethanol in the FFA solution did not exceed 0.5% by volume. The solution was fully dissolved by warming at 37°C for an additional 10 min. The final ratio of FFA/BSA was 2:1. Vehicle

ASBMB JOURNAL OF LIPID RESEARCH

control treatments were prepared using stocks of 10% w/w BSA with an equivalent volume of ethanol added to match that contained in the final FFA stock. The final concentration of ethanol was <0.2% in all experiments.

Cell culture

Rat hepatoma cells, H4IIEC3 (ATCC), were cultured in low-glucose DMEM supplemented with 10% fetal bovine serum and 1% penicillin/streptomycin/glutamine (2 mM). Measurements were done at 70–80% confluency.

Primary hepatocyte isolation and culture

Sprague Dawley rats were purchased from Jackson Laboratories (Bar Harbor, ME) and housed in temperature- and humidity-controlled environment with 12:12 h light-dark cycle and fed standard chow diet ad libitum. Following a 1-week acclimation period, rats were used for primary hepatocyte isolation. Briefly, the hepatic cells of 5- to 6-week-old rats were isolated using collagenase perfusion and first incubated in DMEM-based attachment media containing 20 mM glucose, 100 nM dexamethasone, and 5 nM insulin on collagen IV-coated plates for 4 h (attachment period). The cells were washed once with PBS, and the medium was changed to a DMEM-based growth medium containing 20 mM glucose, 100 nM dexamethasone, and 1 nM insulin for 16 h. Experimental treatments were performed after this period using the same growth medium. All experimental protocols were approved by the Animal Care and Use Committee at Vanderbilt University.

JC1 membrane potential measurement

JC1 is a dye that exists in a monomeric form in nonpolarized mitochondria and fluoresces in the green emission (530 nm) spectrum when excited at 485 nm. The dye accumulates in the mitochondria based on the potential that results in formation of dye aggregates. The aggregation shifts the fluorescence to the red emission (590 nm) spectrum when excited at 485 nm. Therefore, the ratio of red/green is determined and represents alterations in the mitochondrial potential between different cells and treatments.

Cell toxicity

Toxicity was assessed using the dead cell dye propidium iodide as described previously (28). Propidium iodide is an intercalating dye that can only permeate dead cells. It becomes highly fluorescent when embedded in the double-stranded DNA exposed after cell death. After culturing cells in 96-well plates with experimental treatments, the medium was removed and replaced with a solution of the dye and serum-free DMEM. Cells were incubated at 37°C for 1 h in the dark prior to the fluorescence measurement at excitation/emission wavelength of 530/645 nm.

Caspase activation

The Apo-ONE Homogenous Caspase 3/7 Assay kit was used to measure apoptotic caspase activation. Cells were cultured in 96-well plates and incubated with desired treatments for 6 h. The Apo-ONE kit uses a lysis buffer combined with a caspase 3/7-specific substrate (Z-DEVD-R110), which becomes fluorescent once these caspases remove its Asp-Glu-Val-Asp (DEVD) amino acid sequence peptide. Fluorescence was measured at excitation/emission wavelength of 485/535 nm.

Western blotting

Cells were lysed with ice-cold RIPA lysis buffer (sc-24948; Santa Cruz Biotechnology Inc.) supplemented with Na-orthovanadate, protease inhibitor cocktail, and PMSF for 30 min on ice. Samples were centrifuged at 16,100 rcf and 4°C for 20 min, and the resulting supernatants constituted the total protein extracts. Protein concentrations were determined by BCA assay (Thermo Fisher Scientific, Rockford, IL). Samples were added in concentrations of 30 μg/lane for SDS-PAGE Western blotting. Dilutions of the primary antibodies were anti-CHOP (1:1,000) and anti-β-actin (1:1,000).

PL FA profiles

Cells seeded in 10 cm petri dishes at an initial density of 4×10^6 cells per plate were incubated in standard medium until reaching ~70–80% confluency, at which time experimental treatments were administered. Cells were then trypsinized for 3 min and scraped using cold PBS. Cell suspensions were pelleted by centrifugation and resuspended in fresh PBS. Fatty acyl lipid analysis was performed by the Vanderbilt Hormone Assay and Analytical Services Core using TLC and GC-flame ionization detection (GC-FID) techniques. Briefly, lipids were extracted from the aforementioned cell pellets using a modified Folch separation. An internal standard (1,2-dipentadecanoyl-*sn*-glycero-3-phosphocholine) for PLs was added to the lipid-containing chloroform phase. Total lipids were then extracted and separated by TLC using petroleum ether-ethyl ether-acetic acid (80:20:1, v/v/v) on silica plates. Spots corresponding to PLs, TAGs, and FFAs were visualized with rhodamine 6G in 95% ethanol and scraped individually into glass tubes for transmethylation. Transmethylation was performed using a boron trifluoride-methanol 10% (w/w) solution. Derivatized lipids were then analyzed using a GC-FID, where standardized calibration curves were used to analyze FA content.

[^{3}H]palmitate lipid class incorporation

Cells seeded in 6-well dishes at 1.5×10^6 cells per well were incubated in standard medium until reaching ~70–80% confluency. Next, the cells were incubated for the indicated duration at 37°C in 400 μM [9,10-^{3}H]PA (1 μCi ^{3}H/μmol PA), either in the presence or absence of OA. Lipids were extracted using a modified Folch procedure; twice, 0.75 ml chilled methanol was added to each well, and cells were scraped into 1:1 chloroform-water. Once vortexed and centrifuged, the lipid-containing chloroform phase was vacuum dried without heat. Lipid classes were separated by TLC, as described previously. Each TLC spot was added to an individual vial, and radioactivity was assessed by scintillation counting.

Electron microscopy

Cells were seeded in 10 cm dishes at 4×10^6 cells per dish and incubated in standard medium until reaching ~70–80% confluency. Cells were then incubated with desired treatments at 37°C for the indicated time period and then washed thoroughly with 0.1 M sodium cacodylate buffer (with 1% calcium chloride), pH 7.4. After washing, cells were fixed with a 2.5% glutaraldehyde solution in 0.1 M sodium cacodylate buffer for 1 h at room temperature followed by 23 h at 4°C. Samples were postfixed in 1.25% osmium tetroxide and subsequently stained with 2% aqueous uranyl acetate. Embedded cells were then thin-sectioned and viewed on a Philips/FEI T-12 high-resolution transmission electron microscope.

Quantification of electron micrographs

Images produced from electron microscopy were loaded into the publicly available software program Image J. The straight-line measurement function of this program was used to determine the relative length of the scale bar (in nanometers) embedded in the image. Four randomly selected images from each treatment type were then quantitatively analyzed by measuring 10 points on the ER membranes displayed (n = 10/image). The relative ER

widths of these data points could then be converted to an absolute value (in nanometers) using the relative ratio multiplicative factor determined by measuring the scale bar. Once converted to an absolute value, all data points from the respective treatments were pooled together to calculate the mean and SE.

PL analysis

H4IIEC3 cells were grown in 6 cm dishes and treated with the indicated FA(s) for 12 h before they were pelleted and immediately snap frozen using liquid nitrogen. Glycerophospholipids were extracted using a modified Bligh and Dyer procedure (29, 30). Briefly, each pellet was homogenized in 800 μl of ice-cold 0.1 N HCl/CH_3OH (1:1) by vortexing for 1 min at 4°C. Suspension was then vortexed with 400 μl of ice-cold $CHCl_3$ for 1 min at 4°C, and the extraction proceeded with centrifugation (5 min, 4°C, 18,000 *g*) to separate the two phases. Lower organic layer was collected and solvent evaporated. The resulting lipid film was dissolved in 100 μl of isopropanol/hexane/100 mM NH_4COOH(aq) 58:40:2 (mobile phase A). Quantification of glycerophospholipids was achieved by the use of an LC/MS technique using synthetic odd-carbon diacyl and lysophospholipid standards. Typically, 200 ng of each odd-carbon standard was added per sample. Glycerophospholipids were analyzed on an Applied Biosystems/MDS SCIEX 4000 Q TRAP hybrid triple quadrupole/linear ion trap mass spectrometer (Applied Biosystems, Foster City, CA) and a Shimadzu high-pressure LC system with a Phenomenex Luna Silica column (2 × 250 mm, 5 μm particle size) using a gradient elution as previously described (30, 31). The identification of the individual species, achieved by LC/MS/MS, was based on their chromatographic and mass spectral characteristics. This analysis allows identification of the two FA moieties but does not determine their position on the glycerol backbone (*sn-1* vs. *sn-2*). Therefore, glycerophospholipids species are referred to throughout using X:Y notation (X is the total number of carbon atoms, and Y is the total number of double bonds in both FAs, e.g., 36:1 PC).

Neutral lipid analysis

Neutral glycerolipids [monoacylglycerol (MAG), DAG, and TAG] were extracted by homogenizing cell pellets in the presence of internal standards (300 ng each 14:0 MAG and 24:0 DAG, and 600 ng 42:0 TAG) in 2 ml 1× PBS and extracting with 2 ml ethyl acetate-trimethylpentane (25:75). After drying the extracts, the lipid film was dissolved in 1 ml hexane-isopropanol (4:1) and passed through a bed of silica gel 60 Å to remove remaining polar PLs. Solvent from the collected fractions was evaporated, and lipid film was redissolved in 90 μl 9:1 $CH_3OH/CHCl_3$, containing 10 μl of 100 mM CH_3COONa for MS analysis essentially as described (32).

Statistical analysis

All data are represented as mean ± SE. Type I ANOVA (Student's *t*-test) was used to assess statistical differences involving multiple (two) treatments. ANOVA was followed with Tukey-Kramer post hoc testing for ^{3}H-labeled PA experiments.

RESULTS

Treatment of hepatocytes with the SFA PA is associated with perturbations in ER morphology and organelle stress

We hypothesized that the lipotoxic effects of PA could be mainly attributed to its ability to destabilize the structure and function of key organelles, specifically the ER. Increased saturation of PL species has been previously associated with stiffening of cellular membranes (24, 33) and organelle dysfunction (13, 34). Therefore, we sought to examine the effect that FA treatments have on the structure and morphology of hepatic cellular organelles. We were particularly interested in the impacts on the ER membrane because the ER constitutes more than half of total membrane content in hepatocytes and smooth ER is the major site of cellular PL biosynthesis (35, 36). Furthermore, ER stress has been implicated as a critical mediator in the PA-induced lipoapoptotic cascade (8, 13, 21) and is involved in diseased states such as obesity (22, 37) and progressive liver disease (38, 39). The morphology of this organelle appears normal in TEM images of vehicle-treated cells, with tubular cisternae studded by the electron-dense dots characteristic of attached ribosomes (**Figs. 1A**, **2A**). In contrast, both primary hepatocytes and H4IIEC3 cells treated with 400 μM PA for 12 h and 4 h, respectively, exhibited distended ER structures that were dramatically increased in size relative to those of vehicle-treated cells (Figs. 1B, 2B). Quantification of ER expansion revealed that its average thickness increased significantly in cells treated with PA compared with vehicle-treated cells (primary hepatocytes: 40.22 ± 2.93 nm vs. 24.59 ± 1.00 nm, $P < 0.01$, Fig. 1E; H4IIEC3: 64.08 ± 2.39 nm vs. 25.79 ± 0.90 nm, $P < 0.01$, Fig. 2E). The drastic dilation in ER morphology is indicative of ER stress and dysfunction in PA-treated cells (40). There does not appear to be any indication of significant changes in mitochondrial structure between treatments at this time point.

Neither primary hepatocytes nor H4IIEC3 cells treated with 400 μM OA experienced any significant changes in ER morphology compared with vehicle-treated cells, despite carrying the same FA load as those treated with PA alone (Figs. 1C, 2C). Quantification of ER thickness revealed no significant differences between OA- and vehicle-treated primary hepatocytes (23.6 ± 0.64 nm vs. 24.59 ± 1.00 nm, Fig. 1E) or H4IIEC3 cells (25.63 ± 0.77 nm vs. 25.79 ± 0.90 nm, Fig. 2E). OA-treated cells, conversely, did demonstrate significant increases in lipid droplet accumulation, composed primarily of TAGs, compared with those treated solely with PA, as indicated by the white, spherical droplets appearing on the electron micrographs (labeled "LD"). Coincubation of PA-treated cells with 400 μM OA reversed the distended ER morphology observed in cells exposed to PA alone; the ER structure of these cotreated cells closely resembled that of control cells both in terms of visual morphology (Figs. 1D, 2D) and quantified thickness (Figs. 1E, 2E) in both primary hepatocytes and H4IIEC3 cells, respectively. All other subcellular structures appear normal and similar at this time point among all treatment groups. Taken together, there is clearly a substantial difference in ER morphology between hepatic cells treated with SFAs versus MUFAs. Additionally, the structural changes in the ER associated with PA exposure can be completely reversed by cotreatment with OA.

Changes in levels of ER stress markers associated with PA, but not PA + OA cosupplementation, closely followed trends in ER morphological alterations corresponding to the same treatments in H4IICE3 cells. We used CHOP/

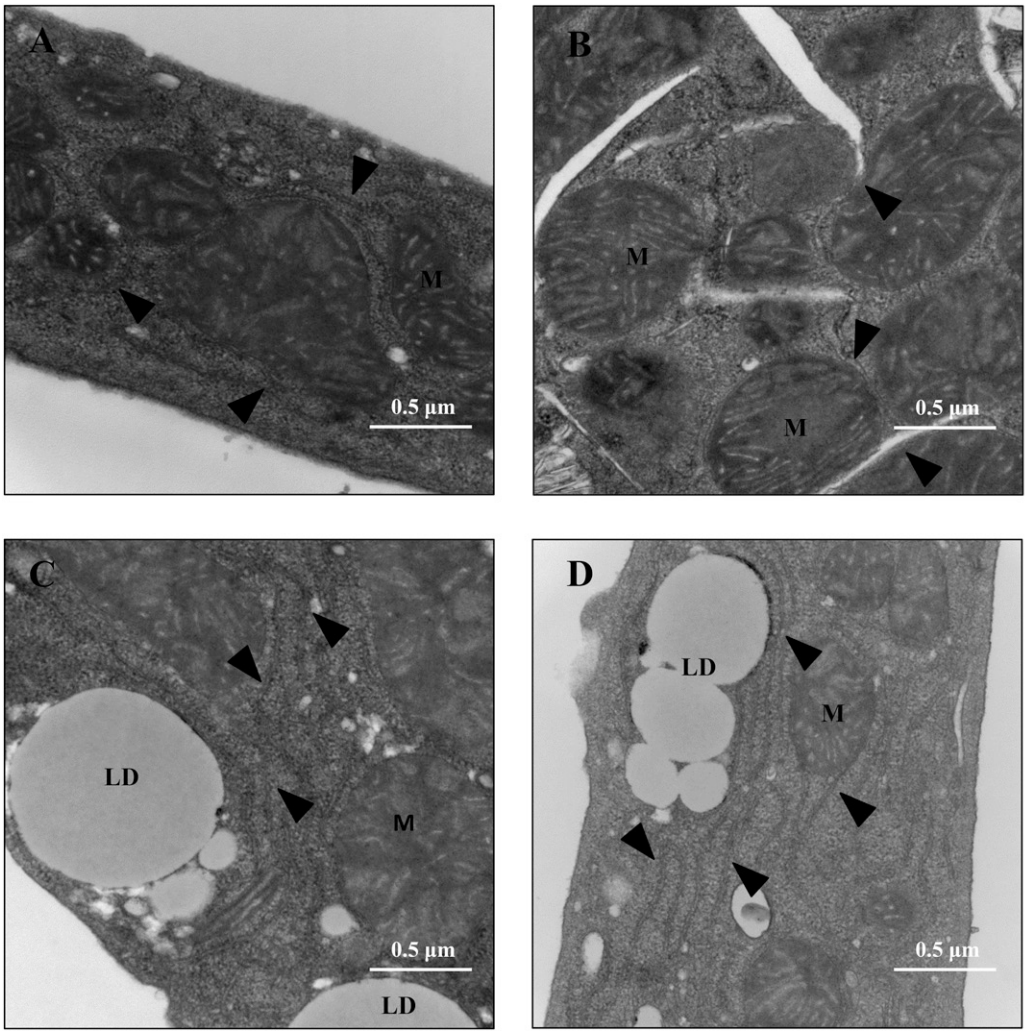

E.

Fig.	Treatment	Average ER diameter ± SE (nm)
1A	BSA	24.59 ± 1.00
1B	PA	40.22 ± 2.86[b]
1C	OA	23.60 ± 0.64
1D	PA+OA	22.87 ± 0.65

Fig. 1. Incubation of freshly isolated primary hepatocytes with PA results in expansion of the ER membrane while cotreatment with OA blocks PA-induced dilation. Primary hepatocytes were incubated for 12 h with BSA vehicle (A), 400 µM PA (B), 400 µM OA (C), or 400 µM PA + 400 µM OA (D). Changes in ER morphology were observed by high-resolution imaging with TEM. Arrowheads point toward ER cisternae. LD, lipid droplets; M, mitochondria. Average ER diameter was quantified using ImageJ length analysis, and results are displayed in E. Scale bars = 500 nm; [b] $P < 0.01$ versus cells treated with BSA.

GADD153 as a marker of ER stress due to its known function as a proapoptotic protein upregulated during the ER stress response. Based on a time course of CHOP protein levels (supplementary Fig. IIIA), 8 h was determined as an optimal point for assessing differences in CHOP expression in response to PA treatment. The intensity of CHOP expression increased in a concentration-dependent manner at 8 h (supplementary Fig. IIIB), similar to the increases in cell death (supplementary Fig. IA). At this time point, H4IIEC3 cells treated with PA demonstrated significantly increased levels of CHOP, indicating substantial upregulation of UPR and confirming that ER stress is associated with PA-induced lipotoxicity (**Fig. 3**). This response was completely reversed by the addition of OA, a representative Western blot of which is shown in Fig. 3.

OA cosupplementation modifies PA partitioning into intracellular lipid pools

Due to the dramatic and differential effects that PA and OA had on ER structure and function, we sought to assess the consequences of PA treatment on intracellular lipid flux. There are two possible mechanisms by which OA could restore normal PL saturation: *i*) by sequestering PA flux away from PL synthesis and into alternate lipid pathways or *ii*) by competing with PA for esterification into the PL pool. We first examined the partitioning of [^{3}H]PA into the five main classes of cellular lipids: PLs, DAGs, FFAs, TAGs, and cholesteryl esters. These data confirm that PL and TAG are the two major fates of exogenous PA, with DAGs also prominent in primary hepatocytes. Primary hepatocytes treated with only PA incorporated ~22% of the exogenous PA into the PL fraction (**Fig. 4A**). The addition of 100 µM and 400 µM OA significantly reduced the PA incorporation into PLs after 24 h by ~50% and 64%, respectively (~11.6% total PA in PL with the addition of 100 µM OA and ~7.9% with 400 µM OA versus 21.9% with PA treatment alone). The redistribution of PA appeared to mainly be channeled toward incorporation into the TAG fraction. In H4IIEC3 cells treated for 12 h with PA alone, ~36% of intracellular PA was partitioned

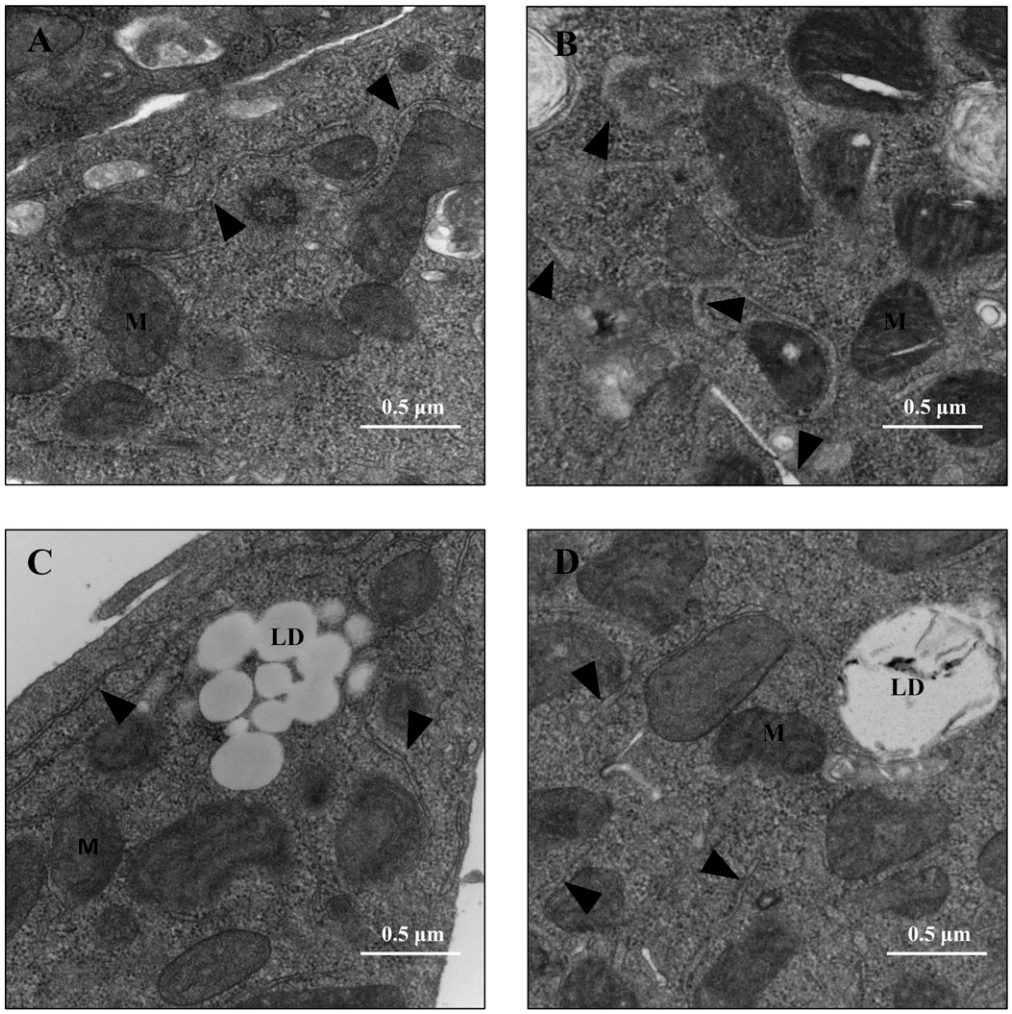

E.

Fig.	Treatment	Average ER diameter ± SE (nm)
2A	BSA	25.79 ± 0.90
2B	PA	64.08 ± 2.93[b]
2C	OA	25.63 ± 0.77
2D	PA+OA	26.08 ± 0.84

Fig. 2. Incubation of H4IIEC3 cells with PA results in expansion of the ER membrane while cotreatment with OA blocks PA-induced dilation. H4IIEC3 were incubated for 4 h with BSA vehicle (A), 400 µM PA (B), 400 µM OA (C), or 400 µM PA + 400 µM OA (D). Changes in ER morphology were observed by high-resolution imaging with TEM. Arrowheads point toward ER cisternae. LD, lipid droplets; M, mitochondria. Average ER diameter was quantified using ImageJ length analysis, and results are displayed in E. Scale bars = 500 nm; [b] $P < 0.01$ versus cells treated with BSA.

into PLs, with nearly all of the remainder incorporated into TAGs (Fig. 4B). Additionally, because primary hepatocytes and H4IIEC3 cells achieved similar degrees of gross phenotype and cellular dysfunction based on analysis of TEM images at differing times (Figs. 1, 2, respectively), it is not surprising that molecular partitioning processes achieve similar scales of change at different times shown in Fig. 4A, B.

As we hypothesized, cosupplementation with OA resulted in a concentration-dependent reduction in PA incorporation into PLs and a corresponding increase in its TAG esterification in both primary hepatocytes and H4IIEC3 hepatic cells. Thus, in the presence of PA alone, hepatic cells incorporated a higher percentage of exogenous PA into structural and signaling PLs than cells cosupplemented with OA. The addition of OA partially redirected the fate of exogenous PA away from PLs and toward incorporation into the more biologically inert TAGs.

PA is rapidly incorporated into cellular PLs and alters the composition of the PL pool

Due to the effects of OA treatment in modifying the intracellular partitioning of PA into different lipid pools and reversing PA-induced lipotoxicity, we evaluated the consequences of PA treatment on total cellular PL composition. The relative percentage of saturated acyl chain substituents on cellular PLs was found to increase significantly within 1 h of exogenous PA treatment in H4IIEC3 cells. The increase in PA incorporation was especially striking; in PA-only treated cells, there was more than a 50% increase in percent total composition PA in the PLs of the PA- versus vehicle-treated hepatomas within the first hour (**Table 1**). This increase in PA incorporation came mainly at the expense of monounsaturated 18:1 moieties, which were significantly reduced under PA treatment. These data indicate that treatment with 400 µM PA leads to rapid incorporation of exogenous PA into cellular PLs, resulting in increased PL

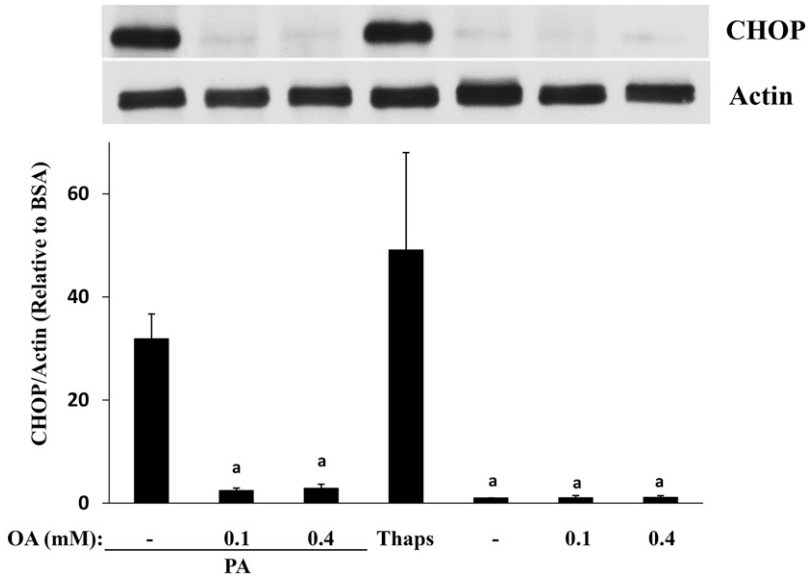

Fig. 3. PA-induced increases in CHOP expression were completely reversed by cotreatment with OA. H4IIEC3 were treated with 400 μM PA with or without OA supplementation for 8 h. Levels of CHOP expression were assessed using Western blotting techniques and quantified with ImageJ densiometric analysis. Representative blot (upper panel); quantification of CHOP/actin (lower panel). Thapsagargin (Thaps) was used as a positive control. Data represent mean ± SE of n = 3. [a] $P < 0.05$ versus cells treated with PA.

saturation. After 6 h (**Table 2**) and 12 h (supplementary Table I), the percentage of PA-containing PLs continued to steadily climb in PA-treated cells. By 12 h, PA comprised ~43% of all PL FAs in PA-treated cells (supplementary Table I) compared with only ~13% in those treated with vehicle (BSA). These changes in cellular PL composition were closely associated with the onset of PA-induced decreases in mitochondrial membrane potential, apoptotic caspase activation, and cell death (supplementary Figs. I, II).

OA cosupplementation partially restores normal PL composition

We further conjectured that OA cotreatment would reverse PA-induced lipoapotosis by alleviating the oversaturation of PL membrane species. Therefore, we examined the effects of cosupplementing PA with OA at various ratios. We found that H4IIEC3 cells cosupplemented with OA incorporated significantly less PA into PLs after 1 h of treatment (Table 1) and demonstrated substantial reductions in relative PA abundance after both 6 and 12 h (Table 2, supplementary Table I), which was accompanied by recovery of relative OA abundance back to levels approaching the vehicle-treated controls by 12 h. In particular, cotreatment with 100 μM or 400 μM OA for only 6 h reduced PA abundance by ~25% and 33%, respectively, while overall PL saturation was reduced similarly by ~16% and 25%, respectively (Table 2). This significant drop in total saturation was mainly attributable to differences in the percentage of palmitic (16:0), palmitoleic (16:1), and oleic (18:1w9) fatty acyl components. Restoration of cellular PL composition was closely associated with a reversal of PA-induced lipotoxicity markers (supplementary Figs. I, II).

PA treatment increases de novo lipid biosynthesis resulting in changes in DAGs and PLs while OA supplementation ameliorates these changes by increased esterification into TAGs

Additionally, we analyzed hepatic cells treated with defined FA supplements in order to quantify the distribution of both neutral and phospholipids at 12 h. H4IIEC3 hepatic cells treated with PA show significantly increased levels of 16:0 LPA (**Fig. 5A**) and both total and 16:0-containing PtdOH (Fig. 5B), specifically 32:0 PtdOH (supplementary Fig. VB), suggesting augmented de novo lipid biosynthesis through the canonical Kennedy pathway in response to SFA supplementation. PA-treated cells accumulated increased quantities of total and 16:0-containing DAG (Fig. 5D), particularly 32:0 DAG (supplementary Fig. VB), and had significantly higher levels of total PL content, including an almost 2-fold increase in the number of PA moieties contained within the PL pool (Fig. 5C). Additionally, the PA-treated cells were not able to synthesize TAGs as effectively as cells supplemented with equimolar concentrations of the UFA OA (Fig. 5E). Alternatively, cotreatment with OA drastically shifted the incorporation of PA in glycero- and phospholipids. The presence of OA led to a dramatic reversal of PA-induced increases in 16:0 LPA, PtdOH, and DAGs (Fig. 5A, B, D, respectively), particularly PA-containing 32:0 species within these classes (supplementary Figs. IVB, VA). Furthermore, OA supplementation significantly reduced both total and 16:0-containing PLs while simultaneously shifting incorporation of the PA toward TAG synthesis (Fig. 5C, E, respectively).

DISCUSSION

ER stress has been previously identified as a key mediator in the lipoapoptosis of CHO and hepatic cells (8, 13,

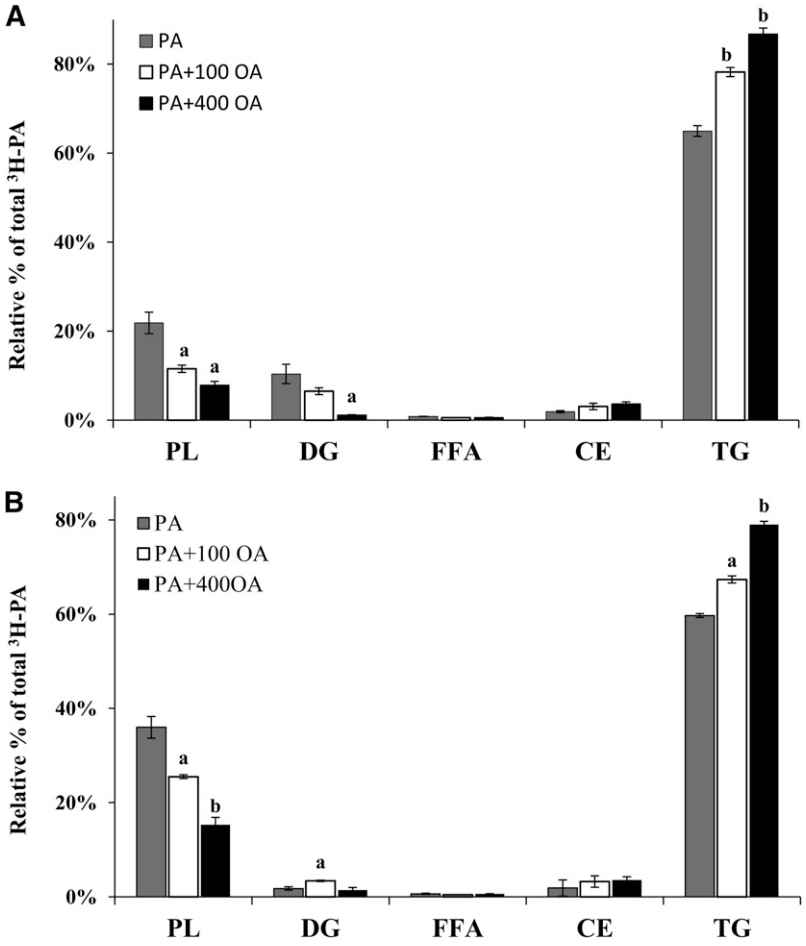

Fig. 4. OA supplementation reduces PA incorporation into PLs while increasing PA incorporation in the TAG fraction. Cells were treated with 400 μM [^{3}H]PA with or without OA supplementation for 24 h in primary hepatocytes (A) or 12 h in H4IIEC3 cells (B). Lipid class incorporation was determined using TLC separation and scintillation counting of each lipid spot. CE, cholesteryl ester; DG; diacylglyceride. Data represent mean ± SE of n = 3. [a] $P < 0.05$; [b] $P < 0.01$ versus cells treated with PA.

21). Other studies have demonstrated that ER stress precedes apoptosis in HeLa cells (34) and hepatic models of lipotoxicity (41). Borradaile et al. (13) found a connection between ER stress and the degree of FA saturation in membrane lipids of CHO cells supplemented with PA. Because the disruption of ER function appears to play an early and critical role in the response to SFA overload, we sought to better understand how lipid metabolism and partitioning of PA into specific lipid classes is affected by OA availability in hepatic cells. We examined the effect that supplementing hepatic cells with PA and OA, alone or in combination, has on lipid metabolism, FA composition of membrane PLs, and particularly on ER function.

Species-level analysis of the PL pool provides insight into mechanistic aspects of lipid synthesis in response to supplementation with differing FAs. Treatment of the H4IIEC3 hepatic cell line with PA resulted in dramatic increases in production of both 16:0 LPA and 32:0 PtdOH,

TABLE 1. PL FA composition of H4IIEC3 cells treated with PA and OA for 1 h (% of total composition)

FA	PA	PA + 100 μM OA	PA + 400 μM OA	BSA	100 μM OA	400 μM OA
14:0	0.65 ± 0.02	0.57 ± 0.01	0.50 ± 0.09	0.72 ± 0.05	0.60 ± 0.05	0.66 ± 0.06
16:0	17.66 ± 0.15	16.33 ± 0.07[a]	15.54 ± 0.63[a]	11.52 ± 0.25[a]	9.75 ± 0.17[a]	10.25 ± 0.08[a]
16:1	5.93 ± 0.11	5.36 ± 0.09[a]	4.99 ± 0.22[a]	5.39 ± 0.18	4.29 ± 0.13[a]	4.45 ± 0.08[a]
18:0	17.24 ± 0.19	16.61 ± 0.12	17.95 ± 0.62	18.33 ± 0.30	16.76 ± 0.14	16.55 ± 0.04
18:1w9	29.88 ± 0.07	32.80 ± 0.09[a]	35.80 ± 0.07[a]	33.11 ± 0.14[a]	39.42 ± 0.34[a]	42.36 ± 0.29[a]
18:1w7	7.56 ± 0.02	7.30 ± 0.01[a]	7.24 ± 0.06[a]	8.44 ± 0.04	7.68 ± 0.02[a]	7.23 ± 0.03[a]
18:2	2.92 ± 0.01	2.80 ± 0.01[a]	2.76 ± 0.03[a]	3.14 ± 0.04[a]	2.83 ± 0.02[a]	2.75 ± 0.01[a]
18:3 w3	0.46 ± 0.01	0.49 ± 0.01[a]	0.00 ± 0.00[a]	0.53 ± 0.02[a]	0.50 ± 0.00[a]	0.20 ± 0.17[a]
20:3w6	0.94 ± 0.01	0.92 ± 0.01	0.85 ± 0.03	0.95 ± 0.02	0.89 ± 0.01	0.79 ± 0.00
20:4	11.75 ± 0.03	11.63 ± 0.10	9.21 ± 0.42[a]	12.48 ± 0.14[a]	11.94 ± 0.10	10.64 ± 0.01[a]
22:5w3	2.06 ± 0.03	2.15 ± 0.04	1.88 ± 0.09	2.21 ± 0.09	2.21 ± 0.03	1.69 ± 0.01
22:6	2.96 ± 0.03	3.04 ± 0.05	2.72 ± 0.14	3.16 ± 0.12	3.14 ± 0.04	2.42 ± 0.02
%SFA	35.54 ± 0.08	33.51 ± 0.13[a]	33.99 ± 0.05[a]	30.58 ± 0.08[a]	27.11 ± 0.03[a]	27.46 ± 0.29[a]
%UFA	64.46 ± 0.02	66.49 ± 0.04[a]	66.01 ± 0.02[a]	69.42 ± 0.04[a]	72.89 ± 0.04[a]	72.54 ± 0.06[a]

H4IIEC3 cells were incubated with 400 μM PA and/or 100 μM or 400 μM OA for 1 h. PLs were separated by TLC and analyzed by GC-FID. Data represent mean FA % ± SE of n = 4.

[a] $P < 0.05$ versus cells treated with PA alone.

TABLE 2. PL FA composition of H4IIEC3 cells treated with PA and OA for 6 h (% total composition)

FA	PA	PA + 100 OA	PA + 400 OA	BSA	100 OA	400 OA
14:0	0.75 ± 0.02	0.66 ± 0.03	0.56 ± 0.07	1.36 ± 0.07[a]	1.13 ± 0.11	0.72 ± 0.05[a]
16:0	35.14 ± 0.42	26.20 ± 0.08[a]	23.32 ± 0.85[a]	13.67 ± 0.16[a]	11.43 ± 0.07[a]	10.29 ± 0.25[a]
16:1	6.83 ± 0.09	6.37 ± 0.06[a]	4.43 ± 0.09[a]	6.09 ± 0.19[a]	4.57 ± 0.08[a]	3.32 ± 0.14[a]
18:0	15.59 ± 0.12	16.63 ± 0.14[a]	14.87 ± 0.47	19.52 ± 0.29[a]	17.26 ± 0.33[a]	16.96 ± 0.24[a]
18:1w9	20.48 ± 0.21	28.82 ± 0.15	37.72 ± 1.06	31.71 ± 0.20	40.80 ± 0.17	48.38 ± 0.16
18:1w7	4.46 ± 0.01	4.44 ± 0.01[a]	3.79 ± 0.07[a]	7.20 ± 0.06[a]	5.85 ± 0.01[a]	4.93 ± 0.01[a]
18:2	1.96 ± 0.00	2.12 ± 0.01[a]	1.95 ± 0.04	2.84 ± 0.08[a]	2.37 ± 0.04[a]	1.87 ± 0.02[a]
20:3w6	0.39 ± 0.23	0.56 ± 0.19	0.23 ± 0.23	0.42 ± 0.24	0.51 ± 0.17	0.54 ± 0.01
20:4	9.72 ± 0.09	9.67 ± 0.07	9.24 ± 0.22	11.85 ± 0.23[a]	11.31 ± 0.24[a]	9.30 ± 0.28
22:4w6	1.16 ± 0.02	1.14 ± 0.03	0.90 ± 0.04[a]	1.26 ± 0.02[a]	0.96 ± 0.03[a]	0.90 ± 0.04[a]
22:5w3	1.49 ± 0.03	1.49 ± 0.03	1.30 ± 0.04[a]	1.78 ± 0.03[a]	1.58 ± 0.05	1.14 ± 0.05[a]
22:6	2.02 ± 0.05	1.91 ± 0.03	1.70 ± 0.07[a]	2.29 ± 0.04[a]	2.24 ± 0.07	1.64 ± 0.08
%SFA	51.48 ± 0.56	43.49 ± 0.26[a]	38.76 ± 1.39[a]	34.55 ± 0.53[a]	29.82 ± 0.51[a]	27.97 ± 0.54[a]
%UFA	48.52 ± 0.72	56.51 ± 0.56[a]	61.24 ± 1.74[a]	65.45 ± 1.09[a]	70.18 ± 0.84[a]	72.03 ± 0.77[a]

H4IIEC3 cells were incubated with 400 μM PA and/or 100 μM or 400 μM OA for 6 h. PLs were separated by TLC and analyzed by GC-FID. Data represent mean ± SE of n = 4.

[a] $P < 0.05$ versus cells treated with PA alone.

strongly suggestive of de novo lipid biosynthesis characteristic of the canonical Kennedy pathway. This was not present in cells cotreated with both PA and OA or those grown in the absence of PA (Fig. 5A and supplementary Fig. IVB, respectively). Specifically, there was a dramatic increase in total PA esterified into PLs and DAGs that was significantly reduced by ~50% with the coaddition of only 100 μM OA (Fig. 5C, D, respectively). In contrast, the cosupplementation with OA resulted in significant increases in PA incorporation into TAGs.

Palmitate treatment has been previously shown to increase DAG species in skeletal muscle models of FFA-induced insulin resistance (42, 43). However, DAG accumulation in our hepatic cell model is secondary to even larger increases in overall PL synthesis, as evidenced by a strong and highly significant increase in both total and PA-containing PLs in cells treated with palmitate alone. This represents a significant finding that provides further context for a potential mechanism in which disordered PL metabolism is the initiator of palmitate-induced ER stress and downstream lipoapoptosis. In addition, observed differences in the molecular species distribution within distinct glycerophospholipid classes, particularly PC, phosphatidylinositol, and phosphatidylserine, are in good agreement with results from a preclinical study of human liver samples from steatotic, cirrhotic, and normal patients (supplementary Figs. IVC, G, H, respectively) (44). Such agreement provides evidentiary support for utilizing hepatocyte lipotoxicity experiments as models to explore remediation of human NAFLD progression.

High-resolution TEM images of cells visually demonstrate the substantial divergence in cellular response to feeding hepatocytes SFAs versus MUFAs. Supplementing cells with PA had a deleterious effect on the structural integrity of the ER membrane of both H4IIEC3 cells and primary hepatocytes after 4 h and 12 h of incubation, respectively, as indicated by obvious dilation of the ER cisternae. This phenomenon has been previously observed in other cell types, specifically CHO (13) and C2C12 muscle cells (45) under similar PA-induced lipotoxic conditions. An identical FA load of OA, however, had no such effect on the ER, and the supplementation of PA-treated cells with OA reversed ER membrane distention and normalized ER morphology. Changes in ER morphology due to FA treatment correlated with augmentation of the ER stress marker CHOP in the presence of exogenous PA (Fig. 3). As with ER dilation and distention, increases in markers of ER stress due to PA treatment were completely reversed by supplementing with OA (Fig. 3).

Changes in ER morphology and function correlated with changes in PA partitioning among lipid classes. PA supplementation resulted in dramatic increases in PA incorporation into PL fatty acyl chains and overall PL saturation (Tables 1, 2 and supplementary Table I). OA cosupplementation reduced PA incorporation into PLs at all examined time points in H4IIEC3 cells (1, 6, and 12 h). This finding is supported by the differential changes in PA partitioning in response to supplementation alone or in combination with OA. We found that under PA/OA cotreatment there was reduced partitioning into the PLs and increased incorporation into the TAG class. These data suggest that the ability of OA to reverse the lipotoxic effects of PA may be tied to its roles in altering the fate of PA away from PL incorporation and toward TAG synthesis and/or in restoring the saturation index of membrane PLs in compositionally sensitive organelles such as the ER.

Overall, our data demonstrate that PA treatment caused increased de novo PL synthesis through the Kennedy pathway, which was not found in hepatocytes cotreated with PA and OA and, to our knowledge, has not been shown previously in models of hepatic lipotoxicity. Furthermore, we observed parallel trends in reversal of apoptotic cell death, Kennedy pathway flux and overall PL saturation, markers of ER stress, and physical ER dilation upon coincubation of PA-treated cells with OA, indicating a strong association between these phenotypic responses. Notably, OA cosupplementation reduced levels of PA in the overall PL composition, which in parallel diminished CHOP expression, ER distention,

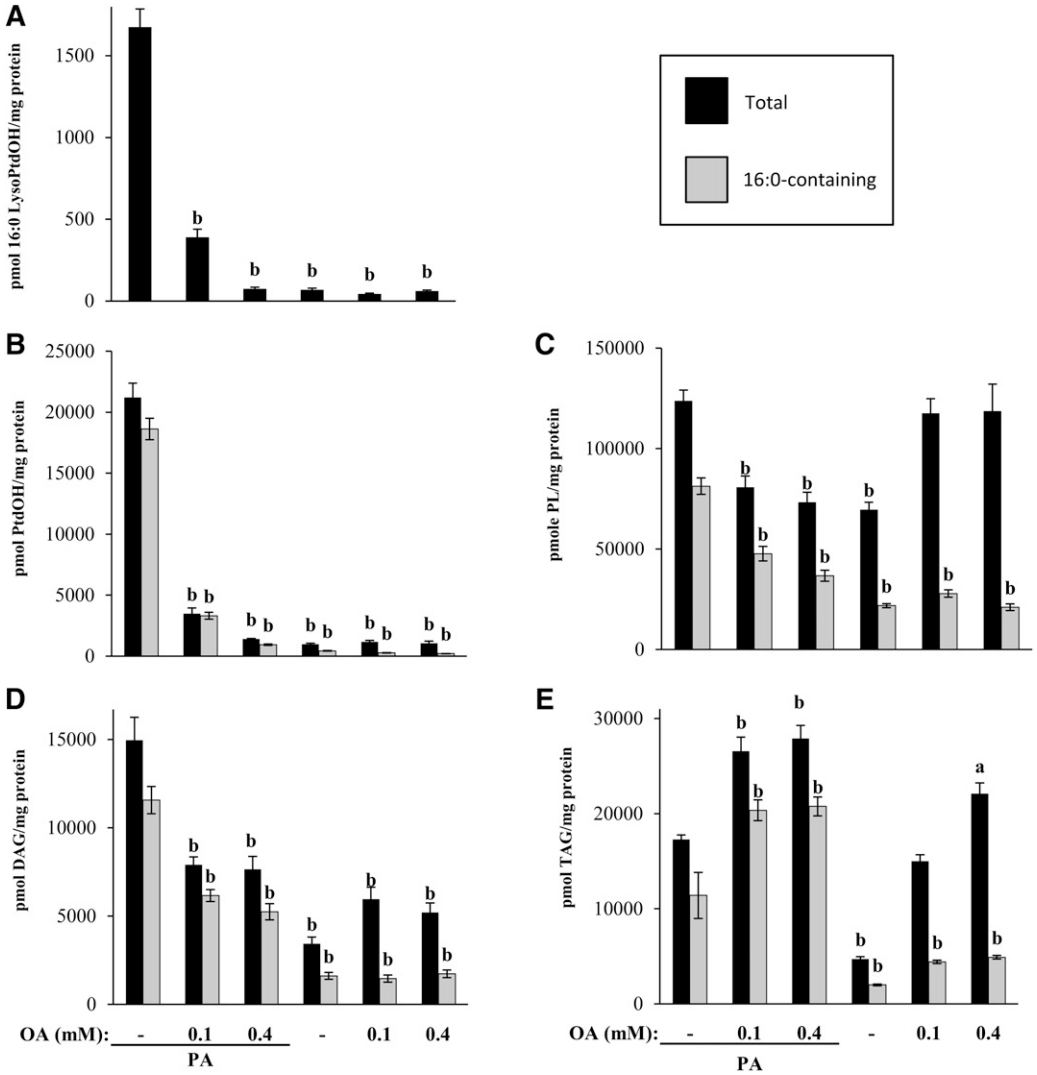

Fig. 5. PA treatment increases 16:0 LPA, PtdOH, PL, and DAG, but not TAG, accumulation. In contrast, cotreatment with OA substantially decreases PL while increasing TAG accumulation. H4IIEC3 cells were treated with 400 μM PA with or without OA supplementation for 12 h. Lipids were determined and quantified using an LC/MS method. Both total and 16:0-containing LPA (A), PtdOH (B), PL (C), and DAG (D) abundance was significantly increased in the presence of PA but was reversed by the addition of OA. Conversely, OA was much more easily incorporated into TAGs than the saturated PA, and cosupplementation with the two FAs synergistically increased overall TG accumulation and 16:0-containing TAGs (E). Data represent mean ± SE of n = 9; [a] $P < 0.05$; [b] $P < 0.01$ versus cells treated with PA.

and reversed PA-induced markers of lipotoxicity in two hepatocyte models. Furthermore, the observed changes in PL composition and ER morphology preceded the onset of mitochondrial dysfunction, as assessed by changes in mitochondrial potential (JC1) and TEM images, as well as caspase activation, suggesting that ER stress may be a critical upstream mediator of the lipotoxic phenotype. This study demonstrates that increased PL saturation is a hallmark and committed step of SFA lipotoxicity in in vitro hepatic models, and that reversing saturation of membrane PLs may have a beneficial effect on hepatic cells exposed to a toxic SFA load. Treatments designed to limit the PL saturation index may point toward novel strategies for improving hepatocyte function under these conditions.

REFERENCES

1. Ibrahim, S. H., R. Kohli, and G. J. Gores. 2011. Mechanisms of lipotoxicity in NAFLD and clinical implications. *J. Pediatr. Gastroenterol. Nutr.* **53:** 131–140.
2. Cazanave, S. C., and G. J. Gores. 2010. Mechanisms and clinical implications of hepatocyte lipoapoptosis. *Clin. Lipidol.* **5:** 71–85.
3. Feldstein, A. E., A. Canbay, P. Angulo, M. Taniai, L. J. Burgart, K. D. Lindor, and G. J. Gores. 2003. Hepatocyte apoptosis and Fas expression are prominent features of human nonalcoholic steatohepatitis. *Gastroenterology.* **125:** 437–443.
4. Cusi, K. 2012. Role of obesity and lipotoxicity in the development of nonalcoholic steatohepatitis: pathophysiology and clinical implications. *Gastroenterology.* **142:** 711–725.
5. Leamy, A. K., R. A. Egnatchik, and J. D. Young. 2013. Molecular mechanisms and the role of saturated fatty acids in the progression of non-alcoholic fatty liver disease. *Prog. Lipid Res.* **52:** 165–174.
6. Noguchi, Y., J. D. Young, J. O. Aleman, M. E. Hansen, J. K. Kelleher, and G. Stephanopoulos. 2009. Effect of anaplerotic fuxes and

amino acid availability on hepatic lipoapoptosis. *J. Biol. Chem.* **284:** 33425–33436.
7. Li, Z. Z., M. Berk, T. M. McIntyre, and A. E. Feldstein. 2009. Hepatic lipid partitioning and liver damage in nonalcoholic fatty liver disease: role of stearoyl-CoA desaturase. *J. Biol. Chem.* **284:** 5637–5644.
8. Wei, Y., D. Wang, C. L. Gentile, and M. J. Pagliassotti. 2009. Reduced endoplasmic reticulum luminal calcium links saturated fatty acid-mediated endoplasmic reticulum stress and cell death in liver cells. *Mol. Cell. Biochem.* **331:** 31–40.
9. Pagliassotti, M., Y. R. Wei, and D. Wang. 2005. Saturated fatty acids induce cytotoxicity in hepatocytes via effects on the endoplasmic reticulum (Abstract). *Obes. Res.* **13:** 31.
10. Listenberger, L. L., X. L. Han, S. E. Lewis, S. Cases, R. V. Farese, D. S. Ory, and J. E. Schaffer. 2003. Triglyceride accumulation protects against fatty acid-induced lipotoxicity. *Proc. Natl. Acad. Sci. USA.* **100:** 3077–3082.
11. Charlton, M., A. Krishnan, K. Viker, S. Sanderson, S. Cazanave, A. McConico, H. Masuoko, and G. Gores. 2011. Fast food diet mouse: novel small animal model of NASH with ballooning, progressive fibrosis, and high physiological fidelity to the human condition. *Am. J. Physiol. Gastrointest. Liver Physiol.* **301:** G825–G834.
12. Listenberger, L. L., D. S. Ory, and J. E. Schaffer. 2001. Palmitate-induced apoptosis can occur through a ceramide-independent pathway. *J. Biol. Chem.* **276:** 14890–14895.
13. Borradaile, N. M., X. Han, J. D. Harp, S. E. Gale, D. S. Ory, and J. E. Schaffer. 2006. Disruption of endoplasmic reticulum structure and integrity in lipotoxic cell death. *J. Lipid Res.* **47:** 2726–2737.
14. Choi, S-E., I-R. Jung, Y-J. Lee, S-J. Lee, J-H. Lee, Y. Kim, H-S. Jun, K-W. Lee, C. B. Park, and Y. Kang. 2011. Stimulation of lipogenesis as well as fatty acid oxidation protects against palmitate-induced INS-1 beta-cell death. *Endocrinology.* **152:** 816–827.
15. Busch, A. K., E. Gurisik, D. V. Cordery, M. Sudlow, G. S. Denyer, D. R. Laybutt, W. E. Hughes, and T. J. Biden. 2005. Increased fatty acid desaturation and enhanced expression of stearoyl coenzyme A desaturase protects pancreatic beta-cells from lipoapoptosis. *Diabetes.* **54:** 2917–2924.
16. Hardy, S., W. El-Assaad, E. Przybytkowski, E. Joly, M. Prentki, and Y. Langelier. 2003. Saturated fatty acid-induced apoptosis in MDA-MB-231 breast cancer cells. A role for cardiolipin. *J. Biol. Chem.* **278:** 31861–31870.
17. Wei, Y., D. Wang, F. Topczewski, and M. J. Pagliassotti. 2006. Saturated fatty acids induce endoplasmic reticulum stress and apoptosis independently of ceramide in liver cells. *Am. J. Physiol. Endocrinol. Metab.* **291:** E275–E281.
18. Srivastava, S., and C. Chan. 2008. Application of metabolic flux analysis to identify the mechanisms of free fatty acid toxicity to human hepatoma cell line. *Biotechnol. Bioeng.* **99:** 399–410.
19. Egnatchik, R. A., A. K. Leamy, Y. Noguchi, M. Shiota, and J. D. Young. 2014. Palmitate-induced activation of mitochondrial metabolism promotes oxidative stress and apoptosis in H4IIEC3 rat hepatocytes. *Metabolism.* **63:** 283–295.
20. Turpin, S. M., G. I. Lancaster, I. Darby, M. A. Febbraio, and M. J. Watt. 2006. Apoptosis in skeletal muscle myotubes is induced by ceramides and is positively related to insulin resistance. *Am. J. Physiol. Endocrinol. Metab.* **291:** E1341–E1350.
21. Pfaffenbach, K. T., C. L. Gentile, A. M. Nivala, D. Wang, Y. R. Wei, and M. J. Pagliassotti. 2010. Linking endoplasmic reticulum stress to cell death in hepatocytes: roles of C/EBP homologous protein and chemical chaperones in palmitate-mediated cell death. *Am. J. Physiol. Endocrinol. Metab.* **298:** E1027–E1035.
22. Fu, S., L. Yang, P. Li, O. Hofmann, L. Dicker, W. Hide, X. Lin, S. M. Watkins, A. R. Ivanov, and G. S. Hotamisligil. 2011. Aberrant lipid metabolism disrupts calcium homeostasis causing liver endoplasmic reticulum stress in obesity. *Nature.* **473:** 528–531.
23. van der Sanden, M. H. M., M. Houweling, L. M. G. van Golde, and A. B. Vaandrager. 2003. Inhibition of phosphatidylcholine synthesis induces expression of the endoplasmic reticulum stress and apoptosis-related protein CCAAT/enhancer-binding protein-homologous protein (CHOP/GADD153). *Biochem. J.* **369:** 643–650.
24. Spector, A. A., and M. A. Yorek. 1985. Membrane lipid-composition and cellular function. *J. Lipid Res.* **26:** 1015–1035.
25. Ron, D., and P. Walter. 2007. Signal integration in the endoplasmic reticulum unfolded protein response. *Nat. Rev. Mol. Cell Biol.* **8:** 519–529.
26. Deguil, J., L. Pineau, E. C. R. Snyder, S. Dupont, L. Beney, A. Gil, G. Frapper, and T. Ferreira. 2011. Modulation of lipid-induced ER stress by fatty acid shape. *Traffic.* **12:** 349–362.
27. Kennedy, E. P. 1987. Metabolism and function of membrane lipids. *Klin. Wochenschr.* **65:** 205–212.
28. Arndt-Jovin, D. J., and T. M. Jovin. 1989. Fluorescence labeling and microscopy of DNA. *In* Methods in Cell Biology. Vol. 30. D. L. Taylor and Y-l. Wang, editors. Academic Press, San Diego, CA. 417–448.
29. Bligh, E. G., and W. J. Dyer. 1959. A rapid method for total lipid extraction and purification. *Can. J. Biochem. Physiol.* **37:** 911–917.
30. Ivanova, P. T., S. B. Milne, M. O. Byrne, Y. Xiang, and H. A. Brown. 2007. Glycerophospholipid identification and quantitation by electrospray ionization mass spectrometry. *Methods Enzymol.* **432:** 21–57.
31. Myers, D. S., P. T. Ivanova, S. B. Milne, and H. A. Brown. 2011. Quantitative analysis of glycerophospholipids by LC-MS: acquisition, data handling, and interpretation. *Biochim. Biophys. Acta.* **1811:** 748–757.
32. Lord, C. C., J. L. Betters, P. T. Ivanova, S. B. Milne, D. S. Myers, J. Madenspacher, G. Thomas, S. Chung, M. Liu, M. A. Davis, et al. 2012. CGI-58/ABHD5-derived signaling lipids regulate systemic inflammation and insulin action. *Diabetes.* **61:** 355–363.
33. Schroeder, F., and E. H. Goh. 1980. Effect of fatty acids on physical properties of microsomes from isolated perfused rat liver. *Chem. Phys. Lipids.* **26:** 207–224.
34. Ariyama, H., N. Kono, S. Matsuda, T. Inoue, and H. Arai. 2010. Decrease in membrane phospholipid unsaturation induces unfolded protein response. *J. Biol. Chem.* **285:** 22027–22035.
35. Alberts, B., A. Johnson, J. Lewis, M. Raff, K. Roberts, and P. Walter. 2002. The endoplasmic reticulum. *In* Molecular Biology of the Cell. 4th edition. Garland Science, New York.
36. Seth, G., P. Hossler, J. C. Yee, and W-S. Hu. 2006. Engineering cells for cell culture bioprocessing – physiological fundamentals. *Adv. Biochem. Eng. Biotechnol.* **101:** 119–164.
37. Özcan, U., Q. Cao, E. Yilmaz, A. H. Lee, N. N. Iwakoshi, E. Özdelen, G. Tuncman, C. Görgün, L. H. Glimcher, and G. S. Hotamisligil. 2004. Endoplasmic reticulum stress links obesity, insulin action, and type 2 diabetes. *Science.* **306:** 457–461.
38. Puri, P., F. Mirshahi, O. Cheung, R. Natarajan, J. W. Maher, J. M. Kellum, and A. J. Sanyal. 2008. Activation and dysregulation of the unfolded protein response in nonalcoholic fatty liver disease. *Gastroenterology.* **134:** 568–576.
39. Özcan, U., E. Yilmaz, L. Özcan, M. Furuhashi, E. Vaillancourt, R. O. Smith, C. Z. Görgün, and G. S. Hotamisligil. 2006. Chemical chaperones reduce ER stress and restore glucose homeostasis in a mouse model of type 2 diabetes. *Science.* **313:** 1137–1140.
40. Xue, X., J. H. Piao, A. Nakajima, S. Sakon-Komazawa, Y. Kojima, K. Mori, H. Yagita, K. Okumura, H. Harding, and H. Nakano. 2005. Tumor necrosis factor alpha (TNF alpha) induces the unfolded protein response (UPR) in a reactive oxygen species (ROS)-dependent fashion, and the UPR counteracts ROS accumulation by TNF alpha. *J. Biol. Chem.* **280:** 33917–33925.
41. Wang, D., Y. R. Wei, and M. J. Pagliassotti. 2006. Saturated fatty acids promote endoplasmic reticulum stress and liver injury in rats with hepatic steatosis. *Endocrinology.* **147:** 943–951.
42. Coll, T., E. Eyre, R. Rodríguez-Calvo, X. Palomer, R. M. Sánchez, M. Merlos, J. C. Laguna, and M. Vázquez-Carrera. 2008. Oleate reverses palmitate-induced insulin resistance and inflammation in skeletal muscle cells. *J. Biol. Chem.* **283:** 11107–11116.
43. Itani, S. I., N. B. Ruderman, F. Schmieder, and G. Boden. 2002. Lipid-induced insulin resistance in human muscle is associated with changes in diacylglycerol, protein kinase C, and I kappa B-alpha. *Diabetes.* **51:** 2005–2011.
44. Gorden, D. L., P. T. Ivanova, D. S. Myers, J. O. McIntyre, M. N. VanSaun, J. K. Wright, L. M. Matrisian, and H. A. Brown. 2011. Increased diacylglycerols characterize hepatic lipid changes in progression of human nonalcoholic fatty liver disease; comparison to a murine model. *PLoS ONE.* **6:** e22775.
45. Peng, G., L. Li, Y. Liu, J. Pu, S. Zhang, J. Yu, J. Zhao, and P. Liu. 2011. Oleate blocks palmitate-induced abnormal lipid distribution, endoplasmic reticulum expansion and stress, and insulin resistance in skeletal muscle. *Endocrinology.* **152:** 2206–2218.